

Computer-Aided Virtual Design of 3-Dehydroquinic Acid Analogues Inhibitors of Dehydroquinase Type II of Mycobacterium tuberculosis with Favorable Pharmacokinetics Profile

DOI: 10.25177/JCCMM.5.3.RA.10774

Research

Accepted Date: 20th Nov 2021; Published Date: 25th Nov 2021

Copy rights: © 2021 The Author(s). Published by Sift Desk Journals Group

This is an Open Access article distributed under the terms of the Creative Commons Attribution License

(http://creativecommons.org/licenses/by/4.0/), which permits unrestricted use, distribution, and reproduction in any medium, provided the original work is properly cited.

Yapi Maxime Yapo^[1], Jocelyne Bosson^[1], Brice Dali^[1], Akoun Abou^[2], Fidele Ntie-Kang^{*,[3,4]}, Mama Nsangou^[4,5] and Luc C. Owono Owono^[4,6]

^[1] Université Nangui Abrogoua, UFR SFA, Laboratoire de Physique Fondamentale et Appliquée, 02 BP 801, Abidjan 02, Côte D'Ivoire

^[2] Institut National Polytechnique Félix Houphouët-Boigny (INPHB), Laboratoire Instrumentation Image et Spectroscopie (L2IS), BP 1093 Yamoussoukro, Côte D'Ivoire

^[3] Department of Chemistry, Faculty of Science, University of Buea, P.O. Box 63, Buea, Cameroon

^[4] Centre for Atomic molecular Physics and Quantum Optics (CEPAMOQ), Faculty of Science, University of Douala, P.O. Box 8580, Douala, Cameroon

^[5] Department of Physics, University of Maroua, P.O. Box 46, Maroua, Cameroon

^[6] Department of Physics, Ecole Normale Supérieure, University of Yaoundé I, P.O. Box 47, Yaoundé, Cameroon

CITATION

Yapi Maxime Yapo, Jocelyne Bosson, Brice Dali, Akoun Abou, Fidele Ntie-Kang, Mama Nsangou, Luc C. Owono Owono, Computer-Aided Virtual Design of 3-Dehydroquinic Acid Analogues Inhibitors of Dehydroquinase Type II of Mycobacterium tuberculosis with Favorable Pharmacokinetics Profile(2021) Journal of Computational Chemistry & Molecular Modeling 5(3) :640-656

CORRESPONDING AUTHOR

Fidele Ntie-Kang

Email: ntiekfidele@gmail.com;

Tel.: +237 685625811

ABSTRACT

New potent 3-dehydroquinic acid (AQs) inhibitors of 3-dehydroquinase dehydratase (dehydroquinase type II) of *Mycobacterium tuberculosis* (MtDHQ2) were obtained by using structure-based molecular design via the *in situ* modification of the template inhibitor AQ1 within the MtDHQ2-AQ1 crystal structure (PDB ID: 2XB8), in order to describe the interactions upon the formation of the complex MtDHQ2-inhibitor.

A training set of 14 AQs with known inhibition constants (K_i^{exp}) was used to establish a quantitative structure-activity relationship (QSAR) model for correlating the $\text{p}K_i^{\text{exp}}$ ($\text{p}K_i^{\text{exp}} = -\log_{10}(K_i^{\text{exp}})$) to the computed Gibbs free energies of formation ($\Delta\Delta G_{\text{com}}$) of MtDHQ2-AQs complexes ($\text{p}K_i^{\text{exp}} = -0.278 \Delta\Delta G_{\text{com}} + 7.653$, $R^2 = 0.98$) is derived. This accounts for the solvent effect and the loss of inhibitor entropy upon enzyme binding. Validation of this QSAR model was performed with 3D-QSAR pharmacophore generation (PH4). The structural information derived from the 3D model and breakdown of computed MtDHQ2-AQs interaction energies up to individual active site residue contribution led to the design of a virtual combinatorial library of 1600 AQs that was screened through the PH4 filter to retain about forty molecules. The absorption, distribution, metabolism and excretion parameters of these designed molecules were computed with the QikProp program while the inhibition constants were predicted by the generated QSAR model. Our computational approach, which combines molecular modeling, pharmacophore generation and analysis of MtDHQ2-AQ interaction energies, resulted in the proposed novel predicted potent antitubercular agents with favorable pharmacokinetic profile, of which the best candidate predicted inhibition constant (K_i^{pre}) value within the picomolar range.

Keywords : *Mycobacterium tuberculosis*; dehydroquinase; QSAR model; pharmacophore model; ADME properties

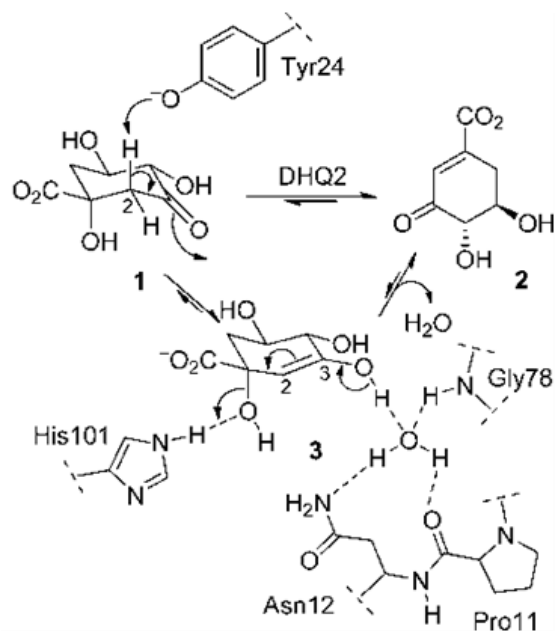
1. INTRODUCTION

It is well known that tuberculosis is a threat to public health worldwide and is, therefore, a major concern for policymakers. In this scope, the World Health Organization (WHO) has set as its next goal the decrease in the incidence of tuberculosis (TB) and TB-related deaths by more than 90% for the 20 years ahead [1]. That target was updated in the meantime to be expected in 2030 while 2020 WHO report stand for 35% [2]. Indeed, due to emerging and rapidly spreading multi-drug resistant and extensively-drug resistant strains of *Mycobacterium tuberculosis* (Mt), the causative agent of TB, this goal will be difficult to achieve without the discovery of new potent antituberculosis drugs. It should be pointed out that despite the increasing worldwide incidence of TB, no novel antituberculosis has been introduced into clinical practice over the past decades. It then becomes of obvious importance to work for the discovery of new drugs against TB. This calls for the urgent diversification of the mycobacterial drug targets in order to fight efficiently against this disease. Among validated *Mycobacterium tuberculosis* targets, attention is driven to enzymes catalyzing vital processes such as dehydroquinase type II (DHQ2) (3-dehydroquinase dehydratase, EC 4.2.1.10) which is involved in the biosynthesis of aromatic amino acids in the mycobacterium [3,4]. Thus the biosynthetic shikimic acid pathway of concern involves seven enzymes that catalyze sequentially the conversion of erythrose-4-phosphate and phosphoenolpyruvate to chorismic acid, a precursor in the synthesis of indispensable compounds such as L-phenylalanine, L-tyrosine, and L-tryptophan, folates, ubiquinone, and vitamins E and K [5,6,7,8]. In addition, the shikimic acid pathway is absent in mammals while it is essential in microorganisms. Consequently, these enzymes are attractive targets for the development of new antimicrobial agents.

Dehydroquinase type II of *Mycobacterium tuberculosis* (MtDHQ2), the third enzyme of this pathway, catalyses the reversible dehydration of 3-dehydroquinic acid (1) to form 3-dehydroshikimic acid (3). This reaction is an anti-elimination which proceeds through a stepwise E1CB mechanism involving an enol intermediate (2) stabilized by a conserved water molecule

[9]. Initially, the tyrosine (Tyr24) removes pro-S hydrogen from C-2 of (1) (Scheme1). The final step is the acid-catalyzed elimination of the C1 hydroxyl group, a reaction mediated by histidine (His101) which acts as a proton donor (scheme 1). Arg19 and Tyr24 have been identified by chemical modification and site-directed mutagenesis studies as key residues for MtDHQ2 activity [10,11]. Both residues belong to a flexible loop that closes over the active site after substrate binding. The essential Arg19 of the loop is presumed to orient the Tyr24 in an appropriate manner for the abstraction of pro-S hydrogen [12,13,14,15,16]

Several research groups have devoted consistent effort towards the discovery of MtDHQ2 inhibitors based on enol intermediate (2) or natural substrate (1) [14,17,18,19,20]. The enol intermediate analogues inhibitors are characterized by the ring flattening due to the π -system formed between the C2-C3 bond and the presence of negative charge at C3 (scheme 1)[20]. In addition, Lorena *et al.* [14] suggested that the inhibition for the enol intermediate analogues depends on the size, the type of aromatic ring and the relative position of the substituent (C2, C3) at the enzyme active site [21,18].



Scheme1: Catalytic mechanism reaction of MtDHQ2. Catalytic residues (Tyr24 initializes abstracting pro-S -hydrogen, His101 finalizes acting as proton donor) and others important are shown

A valuable strategy for *Mt*DHQ2 inhibition is based on the mechanism of reaction which begins with abstraction of the axial proton (C2) of the natural substrate substituting the axial hydrogen by a group able to interact with Tyr24 [1821]. Recent structural and computational studies reported that compounds able to alter the conformation and flexibility of the loop constitute promising candidates for inhibitors of *Mt*DHQ2 [14]. Substitution of either pro-R- or pro-S hydrogen from C2 of natural substrate of the *Mt*DHQ2 by benzyl groups provides potent reversible competitive inhibitors [14,18]. The aromatic ring of these inhibitors establishes strong electrostatic and strong π - π interactions with Arg19 and Tyr24 respectively and consequently reduces the movement of the loop.

In the present work, we have built a QSAR model of *Mt*DHQ2 inhibition for a training set of known AQs analogues [19] that correlates the computed Gibbs free energies of *Mt*DHQ2-AQx complex formation with their observed inhibitory potencies. The point to point QSAR construction has been performed by *in situ* modification of the template inhibitor AQ1 (K_i =26nM) from the crystal structure of *Mt*DHQ2-AQ1 complex (PDB entry: 2XB8) [22].

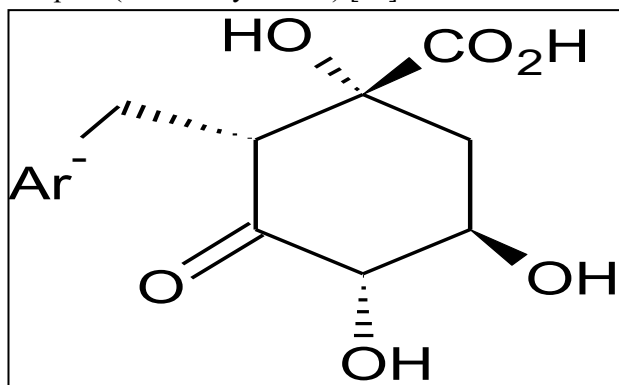


Figure 1. (2R)-2-benzyl-3dehydroquinic acids are reversible competitive inhibitor of *Mt*DHQ2 (substrate analogue)

The robustness of this QSAR model was ascertained by four features of the 3D-QSAR pharmacophore model (PH4), which was prepared using the bound conformations of the training set of AQs. To obtain the desired new and more potent DHQ2 inhibitors analogues, we have built a virtual combinatorial li-

brary of AQs that was screened through the PH4 pharmacophore model in order to identify those analogues that can fit into the mycobacterial DHQ2 binding site. Then, the complexation QSAR model was further used to predict their activities, followed by a selection of the best analogues with the highest predicted inhibitory potencies. Finally, ADME profile of the best-designed analogues was estimated and compared with that of the antitubercular drugs currently used in the clinical practice.

2. MATERIALS & METHODS

The complexation methodology has been described largely according to a process successfully used to elaborate QSAR models of viral, bacterial and protozoal protease-inhibitor complexes and from them to design peptidomimetic, hydroxynaphthoic, thymidine, and triclosan and pyrrolidine carboxamide derivative inhibitors. [23,24,25,26,27,28,29,30,31,32,33,34]. The workflow (Figure 2) describes the steps of whole process of virtual design of novel AQs analogues.

2.1. Training and validation sets

A training set of 14 AQs and a validation set of 3 AQs (Table 1) were selected from a series of compounds with experimentally determined inhibitory activities against DHQ2 of *M. tuberculosis* originating from the same laboratory [19]. The observed activity range K_i^{exp} covers a wide activity range from 26 to 20000 nM, which is sufficient for building a QSAR model of DHQ2 inhibition.

2.2. Model building

The Structure of 3-dehydroquinase dehydratase (dehydroquinase type II) from *Mycobacterium tuberculosis* (DHQ2Mt) in complex with inhibitor compound (2R)-2-(4-methoxybenzyl)-3-dehydroquinic acid (AQ1) has been solved and refined at high resolution (2.40Å) to result in a reference complex DHQ2Mt-AQ1 (Protein Data Bank (PDB) entry code: 2XB8 [30]). Three dimensional (3D) molecular models of enzyme-inhibitor complexes DHQ2 AQx, free enzyme DHQ2 and free inhibitors AQx (where x is an integer from 1 to 14) were constructed from this reference complex DHQ2Mt-AQ1 by *in situ* modification of inhibitor AQ1. The most recent detailed description is in the papers [33,34].

2.3. Molecular Mechanic

Modelling of inhibitors, enzyme and enzyme-inhibitor (E:I) complexes was done in all-atom representation using atomic and charges parameters of CFF91 force field [33]. In all molecular models, a dielectric constant of 4 was employed for all molecular mechanics (MM) calculations in order to take into account the dielectric shielding effect in proteins. The details of this procedure are available in [33,34].

2.4. Conformation search

Conformations of free inhibitors were obtained from the bound conformations in the binary E: I complexes by

gradual relaxation to the nearest local energy minimum. Then a Monte Carlo search (=50,000 iterations) for low-energy conformations was performed over all rotatable bonds, except those in the rings, using Insight II molecular modeling program. Two hundred unique inhibitor conformations were generated by randomly varying torsion angles of the last accepted conformer by $\pm 15^\circ$ at 5000K followed by subsequent energy minimization with a dielectric constant $\epsilon = 80$ to approximate the dielectric screening effect of solvation. The conformer with the lowest total energy was selected and re-minimized at a dielectric constant of 4.

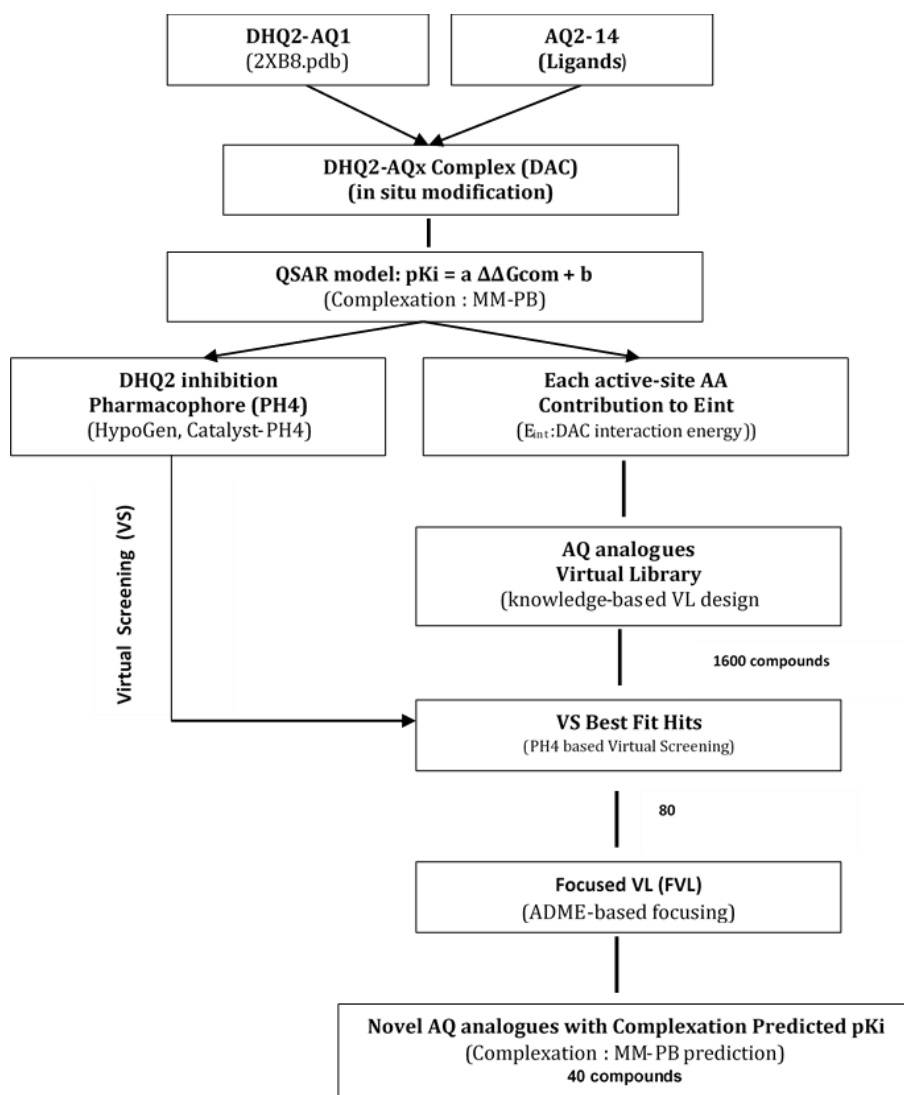


Figure 2. Workflow describing the multistep approach to virtually design novel AQ higher predicted potency against DHQ2

2.5. Entropic term

The vibration entropy change during the inhibitor binding to the enzyme was calculated by normal mode analysis of the inhibitor vibrations using a simplified method of Fischer and al. [35,36]. The most recent details of this procedure were previously described [33, 34].

2.6. Calculation of binding affinity

Calculation of binding affinity establishes the relation between the inhibition constant (K_i) of inhibitor I and the Gibbs free energy change of the formation of E: I complex (ΔG_{com}) in a solvent. This calculation which is based on Molecular Mechanic and Poisson Boltz-

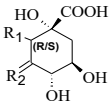
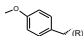
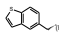
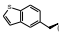
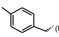
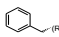
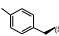
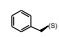

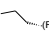
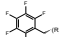
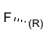
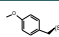
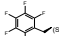
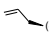
mann scheme is reported fully in references [33, 34]. From this scheme, the final equation which expresses the relative Gibbs free energy changes is:

$$\Delta\Delta G_{\text{com}} = \Delta G_{\text{com}}(\text{I}) - \Delta G_{\text{com}}(\text{I}_{\text{ref}}) = \Delta\Delta H_{\text{MM}} - \Delta\Delta TS_{\text{vib}} + \Delta\Delta G_{\text{sol}}$$

2.7. Pharmacophore generation

Pharmacophore modeling assumes that a set of key structural features responsible for the biological activity of the compound is recognized by the active site during receptor binding. This procedure was reported recently by N. Herman and al. [33] K. Yves and al. [34,34].

Table 1. Training and validation sets of 3-dehydroquinic acid analogues inhibitors (AQ) [21] of dehydroquinase type II (DHQ2) used in the preparation of the QSAR model of inhibitor binding.

			
Training set	$R_1^{a,b}$	R_2^b	$K_i^{\text{exp}}(\text{nM})$
AQ1		O :::::	26
AQ2		O :::::	28
AQ3		O :::::	56
AQ4		O :::::	89
AQ5		O :::::	100
AQ6		O :::::	90
AQ7		O :::::	90
AQ8		O :::::	760
AQ9		O :::::	1700
AQ10		O :::::	47
AQ11		O :::::	8000
AQ12		O :::::	100
AQ13	H -----	HO NH	20000
AQ14	H -----	O :::::	13000
validation set	R_1^a	R_2	$K_i^{\text{exp}}(\mu\text{M})$
AQ15		O :::::	74
AQ16	Br $_{1,4}(\text{R})$	O :::::	15000
AQ17		O :::::	1850

^a Indication of chirality of carbon C2 is in bracket (S) or (R); ^b Dashed bonds indicate the attachment points of the fragments

2.8. Interaction energy

The MM interaction energy (E_{int}) protocol available in DS 2.5[37] computes the non-bonded interactions (van der Waals and electrostatic terms) between enzyme residues and the inhibitor. The calculations were performed using CFF forcefield [38] with a dielectric constant of 4. The breakdown of E_{int} into active-site residue contributions (in % of total E_{int}) reveals the significance of individual interactions and permits a comparative analysis, which leads to the identification of affinity enhancing as well as unfavourable AQ substitutions.

2.9. ADME-Related properties

The ADME properties determine the pharmacokinetic profile of a compound such as octanol/water partitioning coefficient, aqueous solubility, blood/brain partition coefficient, Caco-2 cell permeability, serum protein binding, number of likely metabolic reactions and other eighteen descriptors related to adsorption, distribution, metabolism and excretion of the inhibitors were computed by the QikProp program [39] based on the methods of Jorgensen [40]. The ADME-related properties treatment in this work has been fully described in [33, 34].

2.10. Virtual Combinatorial Library Generation

The analogue model building was performed with Molecular Operating Environment (MOE) program [41]. The library of analogues was enumerated by attaching R-groups (fragments, building blocks) onto AQ scaffold using the Quasar Combi Design module of MOE [41]. Reagents and chemicals considered in this paper were selected from the directories of chemicals available from the commercial sources [[vi]]. Each analogue was built as a neutral molecule in the MOE program [41] and its molecular geometry was refined by MM optimization through smart minimizer of Discovery Studio [37] at high convergence criteria (threshold on energy difference of 10^{-4} kcal.mol⁻¹ and root mean square deviation (RMSD) of 10^{-5} Å) using class II consistent force field CFF [38] described in Molecular Mechanic section, with a dielectric constant of 4.

2.10.1. ADME-based library focusing

The library focusing strategy based on ADME-related properties has been used for the first time in [32].

2.10.2. Pharmacophore-based library focusing

The PH4model described in Section 2.7 was derived

from the bound conformations of the Aqs at the active-site of DHQ2. The enumerated and ADME-focused VL was further focused by using the ligand pharmacophore mapping protocol available of Discovery Studio. Within this protocol, each generated conformer of the analogues was geometry optimized by means of the CFF force field for a maximum of 500 energy minimization steps and subsequently aligned and mapped to the PH4 model in order to select the top ranking overlaps. Twenty best-fitting inhibitor conformers were saved and clustered into 10 conformational families according to their mutual RMSD by Jarvis Patrick complete linkage clustering method. The best representative of each cluster was considered in the virtual screening of analogues. Only those analogues mapping to all four PH4 features were retained for the in silico screening.

2.11. In silico screening

The conformer with the best mapping on the PH4 pharmacophore in each cluster of the focused library subset was selected for in silico screening by the complexation QSAR model. The relative Gibbs free energy (GFE) of the ligand-receptor complex E: I in water $\Delta\Delta G_{\text{com}}$ was computed for each selected new analogue. $\Delta\Delta G_{\text{com}}$ was used to predict the DHQ2 inhibitory potencies (pK_i^{pre}) of the focused virtual library of AQ analogues by inserting this parameter into the target scoring function. This scoring function which is specific for each receptor is parameterized using the QSAR model for the DHQ2 receptor of *M. tuberculosis* by $\text{pK}_i^{\text{pre}}[\text{DHQ2}] = a.\Delta\Delta G_{\text{com}} + b$, where a and b are real numbers.

3. RESULTS

A training set of 14 Aqs and a validation set of 3 Aqs (Table 1) were selected from a series of compounds with experimentally determined activities from the same laboratory [21]. Their inhibitory constants K_i cover a range ($26 \leq K_i \leq 20000$ nM) sufficiently large to enable the building of a reliable QSAR model of MtDHQ2 inhibition.

The relative Gibbs free energies of the enzyme (E),inhibitor (I), complex formation (E:I), were computed for the complexes from *in situ* modification of the template inhibitor AQ1 in the binding site of MtDHQ2 as described in the Methods section.

Table 2. Complexation Gibbs free energy (binding affinity) and its components for the training set of DHQ2 inhibitors AQ1-14 and validation set AQ15-17

Training set ^a	M _w ^b	$\Delta\Delta H_{MM}^c$	$\Delta\Delta G_{sol}^d$	$\Delta\Delta TS_{vib}^e$	$\Delta\Delta G_{com}^f$	$K_i^{exp\ g}$
		(kcal. mol ⁻¹)				(nM)
AQ1	310	0	0	0	0	26
AQ2	336	1.75	-0.47	0.50	0.77	28
AQ3	336	1.70	-0.84	0.13	0.72	56
AQ4	294	2.75	-0.65	-1.14	3.24	89
AQ5	280	3.63	-0.98	-0.15	2.80	100
AQ6	294	-0.23	2.32	0.26	1.83	90
AQ7	280	0.45	2.12	-0.00	2.57	90
AQ8	230	7.79	-0.21	2.28	5.31	760
AQ9	232	7.54	1.45	2.89	6.09	1700
AQ10	370	-2.47	-1.70	-6.95	0.99	47
AQ11	208	9.54	1.08	1.80	8.81	8000
AQ12	310	4.07	-1.39	0.21	2.47	100
AQ13	205	11.03	2.80	2.79	11.05	20000
AQ14	190	9.89	2.44	2.50	9.83	13000
Test set ^a	M _w ^b	$\Delta\Delta H_{MM}^c$	$\Delta\Delta G_{sol}^d$	$\Delta\Delta TS_{vib}^e$	$\Delta\Delta G_{com}^f$	$\frac{pK_i^{pred}}{pK_i^{exp\ h}}$
(kcal. mol ⁻¹)						
AQ15	370	-3.20	-1.24	-5.84	1.40	1.02
AQ16	269	9.61	1.15	0.98	9.78	1.02
AQ17	230	3.15	4.43	1.06	6.51	1.02

^afor the chemical structures of the training set inhibitors see; ^b M_w the molecular mass of inhibitors (g.mol⁻¹); ^c $\Delta\Delta H_{MM}$ is the relative enthalpic contribution to the Gibbs free energy change related to enzyme-inhibitor (E:I) complex formation derived by molecular mechanics (MM): $\Delta\Delta H_{MM} \equiv [E_{MM}\{E: I_x\} - E_{MM}\{I_x\}] - [E_{MM}\{E: I_{ref}\} - E_{MM}\{I_{ref}\}]$, I_{ref} is the reference inhibitor AQ1; ^d $\Delta\Delta G_{sol}$ is the relative solvation Gibbs free energy contribution to the Gibbs free energy change of E:I complex formation: $\Delta\Delta G_{sol} = [G_{sol}\{E:I_x\} - G_{sol}\{I_x\}] - [G_{sol}\{E:I_{ref}\} - G_{sol}\{I_{ref}\}]$; ^e $\Delta\Delta TS_{vib}$ is the relative entropic contribution of inhibitor I_x to the Gibbs free energy related to E:I complex formation: $\Delta\Delta TS_{vib} = [\Delta TS_{vib}\{I_x\} - \Delta TS_{vib}\{I_{ref}\}] - [\Delta TS_{vib}\{I_{ref}\} - \Delta TS_{vib}\{I_{ref}\}]$; ^f $\Delta\Delta G_{com} \equiv H_{MM} + \Delta\Delta G_{sol} - \Delta\Delta TS_{vib}$ is the relative Gibbs free energy change related to E: I_x complex formation; ^g K_i^{exp} is the experimental inhibition constant obtained from reference ^[18]; ^h Ratio of predicted and experimental inhibition constant pK_i^{pre}/pK_i^{exp} ($pK_i^{pre} = -\log_{10} K_i^{pre}$) was predicted from computed $\Delta\Delta G_{com}$ using the regression equation for DHQ2 shown in Table 3.

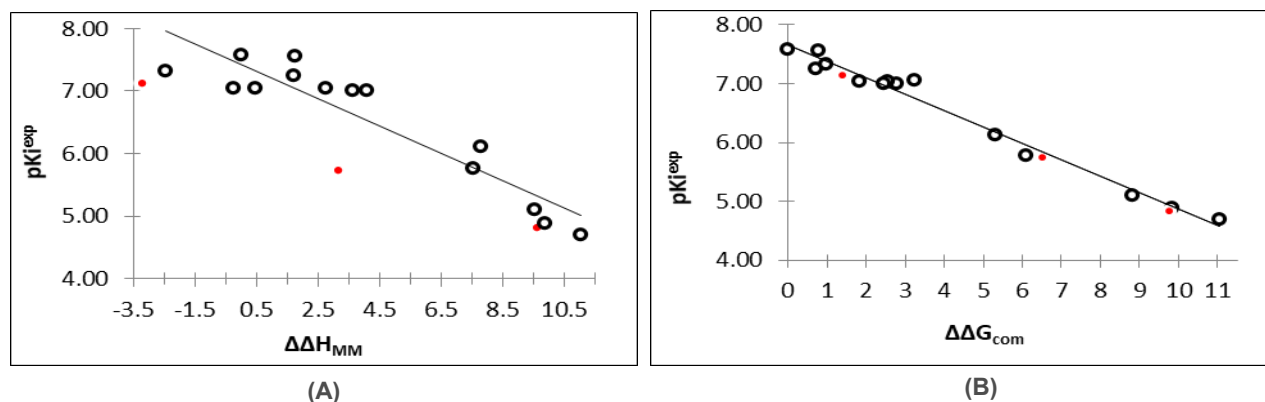


Figure 3. (A): Plot of correlation equation between pK_i^{exp} and relative enthalpic contributions to the Gibbs free energy of DHQ2-AQ_x complex formation of training and validation set. (B): Similar plot between relative complexation Gibbs free energy of DHQ2-AQ_x complex formation $\Delta\Delta G_{com}$ of the training and validation set in kcal.mol⁻¹ and K_i^{exp} . In figures (A and B), training and validation set are plotted in black and red circles respectively.

Table 3. Regression analysis of computed binding affinities $\Delta\Delta G_{\text{com}}$, its enthalpic component $\Delta\Delta H_{\text{MM}}$, and experimental inhibition constant $\text{pK}_i^{\text{exp}} = -\log_{10}(\text{K}_i^{\text{exp}})$ of acid dehydroquinic (AQs) towards MtDHQ2.

Statistical Data of Linear Regression	(A)	(B)
$\text{pK}_i^{\text{exp}} = -0,218 \Delta\Delta H_{\text{MM}} + 7,427$ (A)	-	-
$\text{pK}_i^{\text{exp}} = -0,278 \Delta\Delta G_{\text{com}} + 7,653$ (B)	-	-
Number of compounds	14	14
Square correlation coefficient of Regression R^2	0.86	0.98
LOO cross-validated square correlation coefficient R^2_{xv}	0.85	0.98
Standard error of regression σ	0.39	0.15
Statistical significance of regression,		
Fisher F-test	74.74	623.2
Level of statistical significance α	>95%	> 95%
Range of activities K_i^{exp} (nM)	26 – 20000	

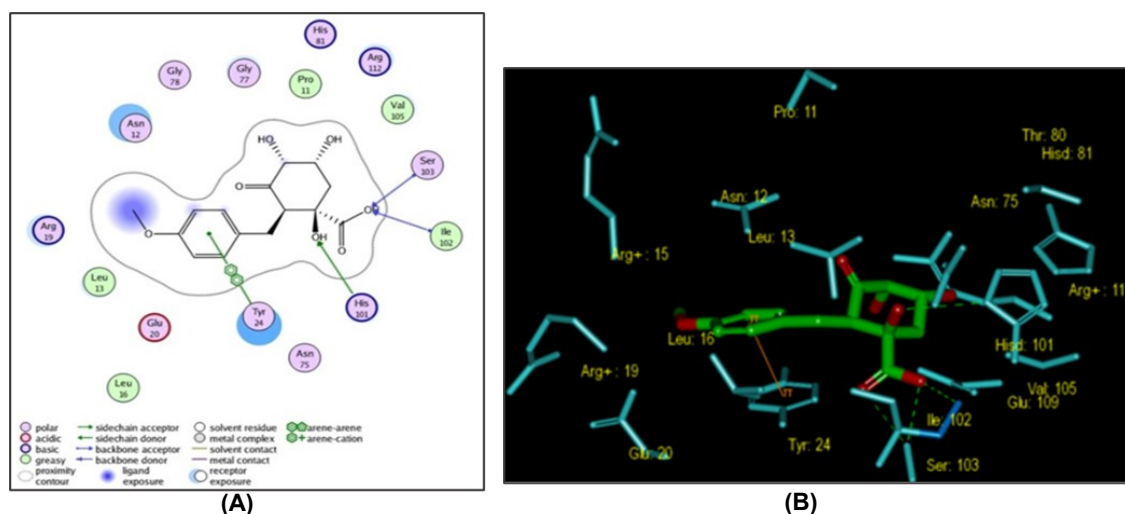


Figure 4. (A) 2D schematic interaction diagram of most potent inhibitor AQ1 [18] at the active site of MtDHQ2; (B) 3D structure of the active site with bound inhibitor AQ1

Table 2 lists the Gibbs free energy and its components. The $\Delta\Delta G_{\text{com}}$ reflects the mutual affinity between the enzyme and the inhibitor. Since it is computed from simulations in an approximate way, the consistency of the binding model is evaluated through a regression analysis leading to linear correlation with experimental activity data (K_i^{exp} [19]). The statistical data of these regressions are illustrated in Erreur ! Source du renvoi introuvable. and listed in Table 3. The relative high values of regression coefficient R^2 and the Fischer F-test of correlation involving $\Delta\Delta G_{\text{com}}$ (eq. B, Table 3), indicate a strong relationship between the binding model and the experimental inhibitory potency (K_i^{exp}) of the series of AQ

as plotted in Figure 3.

The AQ's active conformation from this QSAR is revealed in Figure 4 : (A) 2D schematic interaction diagram of most potent inhibitor AQ1 [18] at the active site of MtDHQ2; (B) 3D structure of the active site with bound inhibitor AQ1 for the most active AQ1. Subsequently, the enzyme-inhibitor relative intermolecular interaction energy (E_{int}) breakdown with their correlation with experimental activity (pK_i^{exp}) was plotted (Erreur ! Source du renvoi introuvable.). A comparative individual residue contribution between the most active AQ1 and less active AQ13 confirms the pK_i^{exp} trend (Figure 6).

The PH4 model derived in the present work, which assumes a set of essential structural features responsible for inhibitor activity was elaborated with the 3D-QSAR pharmacophore protocol of Catalyst HypoGen algorithm implemented in Discovery Studio version 2.5 by using the conformations of inhibitors (AQs) from refined *Mt*DHQ2: AQx complexes. This 3D-QSAR PH4 model was prepared following the usual three steps: constructive step, the subtractive step, and the optimization step. The most active inhibitors ($K_i^{\text{exp}} \leq 2 \times 0.026 \mu\text{M}$) were used to generate the starting PH4 features and the inactive inhibitors served to remove unfavorable features. During the generation of the model, 4 features in the HypoGen algorithm were selected namely hydrophobic aromatic (HYdAr), hydrogen-bond donor (HBD), hydrogen-bond acceptor (HBA) and ring aromatic (Ar) feature. The uncertainty on the biological activity (K_i) was reduced to 1.25 instead of 3. This modification is due to the accuracy and homogeneity of the measured K_i that originated from the same laboratory. The other values of the adjustable parameters were kept. At the end of the procedure, 10 top hypotheses (with their parameters) were generated using a simulated annealing approach (Table 4).

The cost parameters ranging from 48.4 (Hypo1) to 54.7 (Hypo10) attested the reliability of these pharmacophore models. Other statistical data (cost, root-mean-square deviation RMSD, R^2) are listed in Table 4. The PH4 Hypo1 which has the best RMSD and higher R^2 was retained for further analysis. Its regression equation $\text{pK}_i^{\text{exp}} = 1.025 \times \text{pK}_i^{\text{pre}} - 0.123$ is plotted in Figure, and its statistical data ($n=14$, $R^2 = 0.95$, $R^2_{\text{cv}} = 0.94$, F-test = 225.8, $\sigma = 0.238$, $\alpha > 95\%$) attest the predictive capacity of PH4. The Hypo1 which represents a PH4 model with a similar level of predictive power as the complexation GFE *Mt*DHQ2-AQ binding QSAR model may be used to estimate the pK_i of new analogues on the basis of their mapping to its features. The design strategy relied on favorable features such as hydrophobic, hydrogen-bond acceptor, the best PH4 model (Hypo1) and the interactions with residues Asn12, Arg19 and Tyr24.

The virtual library of new 3-dehydroquinic acid com-

pounds with a variety of substitutions in two positions (C2, C3) of 3-dehydroquinic acid was built. During its enumeration, the R- groups listed in Table 5 were attached to R1-R2 of the substrate to generate a combinatorial library of 1600 analogues.

The library of AQ analogues was screened for molecular structures matching to the 3D-QSAR PH4 pharmacophore model Hypo1 of DHQ2 inhibition of *M. tuberculosis*. From the set of 1600 analogues, 80 mapped the 4 features of the PH4, out of which only half best fitting analogues (PH4 hits) were retained and submitted to screening with the complexation QSAR model. Computed Gibbs free energy of complex formation with *Mt*DHQ2 and its components, as well as predicted constant inhibitory estimated from equation (B) are given in Table 2.

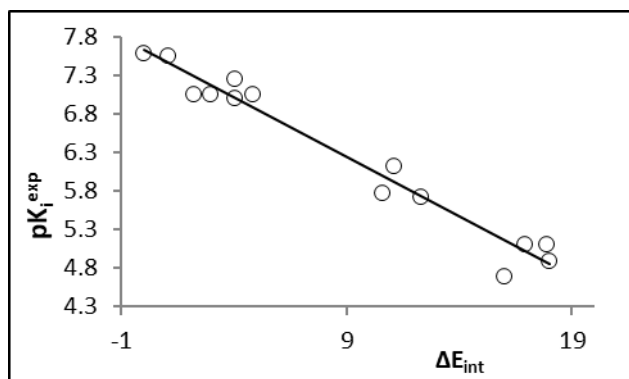


Figure 5. Relative enzyme-inhibitor intermolecular interaction energy plot for training set

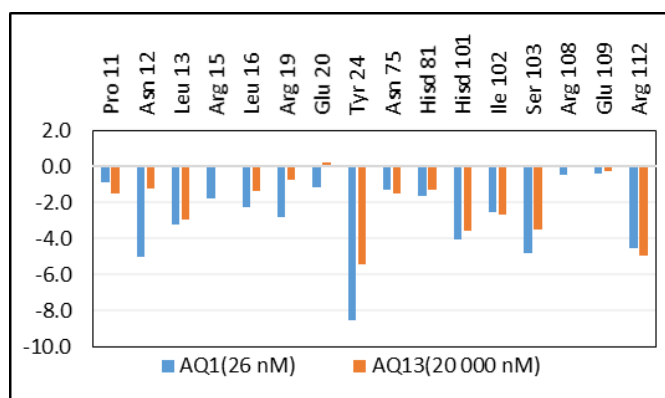


Figure 6. Molecular mechanics interaction energy E_{int} breakdown (in kcal.mol⁻¹) to active site residues contributions for the most active AQ1 and the less active AQ13

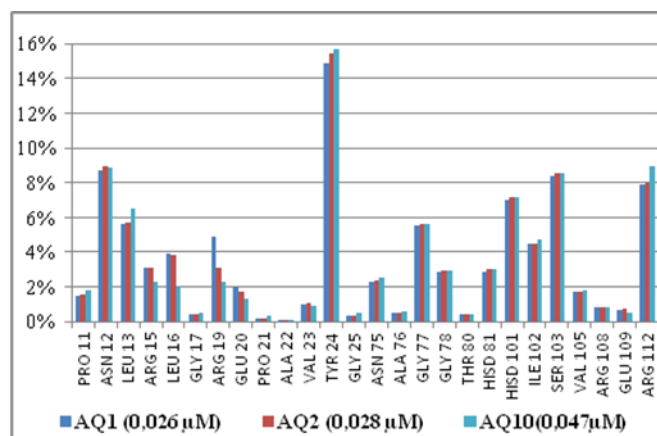


Figure 7. Interaction energy breakdown (in % of the total Eint of MtDHQ2-AQ) to residue contributions for highly active training set Aqs

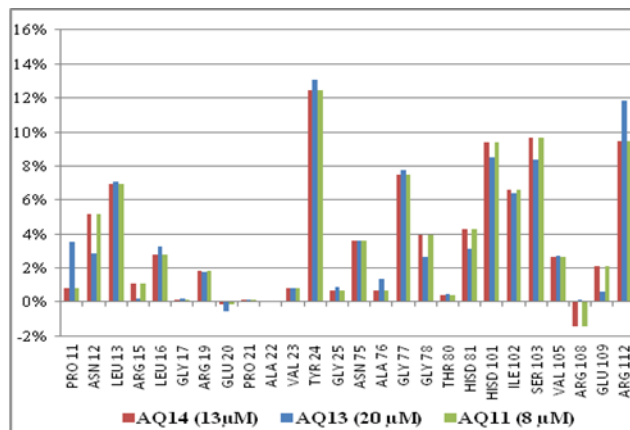


Figure 8. Interaction energy breakdown (in % of the total Eint of MtDHQ2-AQ) to residue contributions for less active training set Aqs

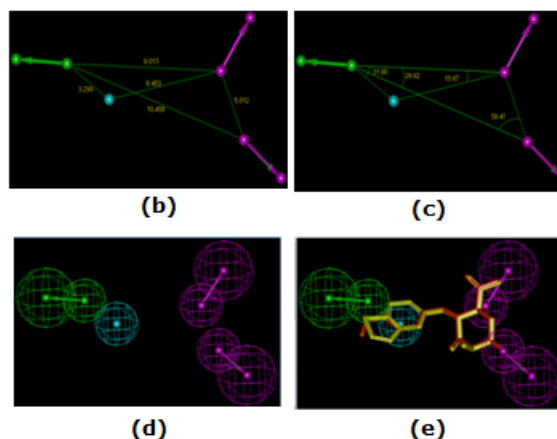
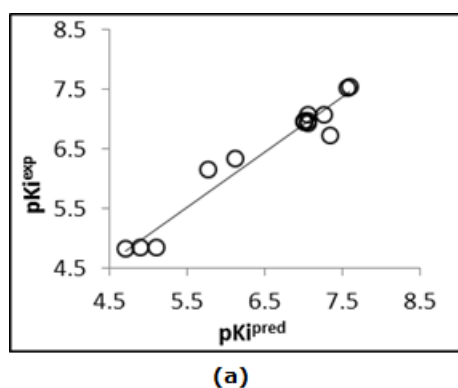


Figure 9. The correlation plot of experimental vs. predicted inhibitory activity (a) Coordinates (b, c), features (d) and mapping (e) of the DHQ2 inhibitors pharmacophore with the best fit hit AQ1 (red), AQ2 (yellow). The features are colored blue for hydrophobic (Hyd), green for hydrogen-bond acceptor (HBA) and purple for the hydrogen-bond donor (HBD). The arrows represent the projection for donor and acceptor features.

Table 4. Output parameters of 10 generated PH4 pharmacophoric hypotheses for DHQ2 inhibitors after Cat-Scramble validation procedure.

Hypothesis	RMSD ^a	R ² ^b	Total Cost ^c
Hypo1	0.829	0.99	48.4
Hypo2	0.767	0.99	48.5
Hypo3	0.671	0.99	49.6
Hypo4	1.005	0.98	50.8
Hypo5	1.133	0.97	51.7
Hypo6	0.973	0.98	51.9
Hypo7	1.041	0.98	52.5
Hypo8	1.107	0.98	53.5
Hypo9	1.182	0.97	54.5
Hypo10	1.195	0.97	54.7
Fixed Cost	0.0	1.00	43.8
Null Cost	4.986	0.00	179.3

^aroot mean square deviation (RMSD); ^bsquared correlation coefficient; ^coverall cost parameter of the PH4 pharmacophore

The new analogues are derived from the most potent training set inhibitor AQ1 (Table 1) and are intended to involve residues Asn12, Arg19 and Tyr24 upon inhibitor binding. The best of them, AQ38-02 reached predicted inhibitory potency towards *MtDHQ2* $K_i^{\text{pre}} = 0.25$ nM (Table 7Erreur ! Source du renvoi introuvable. This best analogue AQ38-02 involves strong interactions with the above-mentioned residues (Figure 11). As an illustration, we can mention σ - π interaction between the side chain of Asn12 and aromatic ring moiety, π - π interaction between the side chain of Tyr24 and aromatic ring moiety and, hydrogen bonding between Arg19 and the oxygen atom of this fragment. In the position R2, the fluorine atom establishes Hydrogen bonding interaction with residue

Asn12 and Gly78. These interactions intensified the affinity towards *MtDHQ2*.

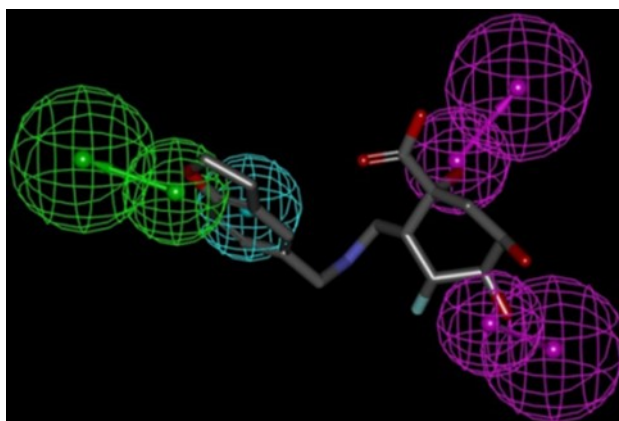
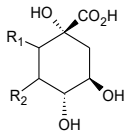


Figure 10. PH4 Mapping of the best fit hit AQ38-02

Table 5. R-groups (fragments, building blocks substituents) used in the design of the initial diversity library of AQ analogues [38].

					
R-groups ^a					
1	...H	2	...F	3	...Cl
4	...CH ₃	5	...OH	6	...SH
7	...CN	8	...NH ₄ ⁺	9	...
10	...NH	11	...N	12	...OH
13	...SH	14	...NH ₃ ⁺	15	...NH
16	...	17	...	18	...
19	...	20	...	21	...
22	...	23	...	24	...
25	...	26	...	27	...
28	...	29	...	30	...
31	...	32	...	33	...
34	...	35	...	36	...
37	...	38	...		
39	...	40	...		

^aDashed bonds indicate the attachment points of the fragments

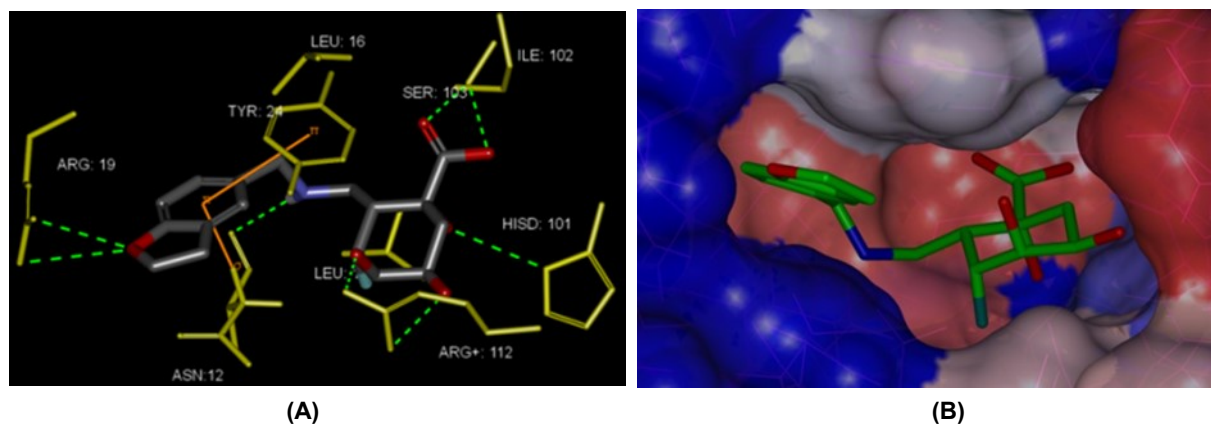


Figure 11. (A) Interactions of the most potent designed analogue AQ38-2 (Table 8) at the active site of MtDHQ2. The active site residues contributing the most to the Inhibitor binding are shown. HBs are shown as dash green and π - π interactions are shown as a solid orange line. (B) Connolly surface of the predicted most active AQ38-2 at the active site DHQ2Mt. The binding cleft surface is colored according to residue hydrophobicity: red-hydrophobic, blue-hydrophilic and white intermediate residues

Table 6. Molecular mechanics interaction energy Eint (in kcal.mol⁻¹) for epimers (2R/2S).

R	epimer	Eint (kcal.mol ⁻¹)
	R	-57.45
	S	-54.30
	R	-56.39
	S	-53.45
	R	-55.27
	S	-54.49
	R	-53.44
	S	-52.64

4. DISCUSSION

QSAR model of dehydroquinase type II of *M.tuberculosis* (DHQ2Mt) inhibition was built revealing the AQ active conformation. Then a 3D-QSAR pharmacophore (PH4) model of DHQ2Mt inhibition of bound AQ conformations was elaborated. The PH4's predictability served to screen a virtual combinatorial library of AQ analogues with the aim

to design more potent DHQ2Mt inhibitors.

4.1. QSAR model

The effectiveness of this one descriptor QSAR model is assessed through the components of GFE ($\Delta\Delta\Box_{com}$) namely the enthalpic $\Delta\Delta H_{MM}$, solvation $\Delta\Delta G_{solv}$ and entropy variation ($\Delta\Delta TS$) of the inhibitor upon binding. The relevance of the enthalpic contribution to GFE is well illustrated by the quality of the regression indicating that in gas phase a large part (some 86%) of the variation of the pK_i^{exp} is explained by that of H_{MM} . Adding to the first component of the solvation contribution in order to come closer to the biological medium, kept the level of strong relationship between the experimental data and the simulation results. Finally the likeliness of the model is increased by the loss of the inhibitor vibrational entropy upon binding TS_{vib} to explain some 98% of the variation of pK_i^{exp} by that of GFE. The differences in inhibition potencies between the 2R- and the 2S-substituted derivatives are verified in Table 6; 2R-substituted derivatives are more potent in general according to the results of Lorena T. and al. [14]. A comparative enzyme-inhibitor intermolecular interaction energy between 2R- and 2S-substitutes confirms the activity trend.

Relatively high values of the squared regression coefficients and Fischer F-test show strong correlation

between the binding models computed quantities ($\Delta\Delta H_{MM}$ and $\Delta\Delta G_{com}$) and the experimental inhibitory potencies of the series of AQs. Thereafter, equation (B) will be used to evaluate the inhibition constants pK_{ipre} of the molecules of the validation set. The ratio of the predicted and the observed inhibitory potencies (pK_{ipre}/pK_{iexp}) for the validation set of AQs (not included in the training set) is close to one (Table 2), showing the reliability of the QSAR model. Therefore, the complexation QSAR correlation Equation (B) and computed $\Delta\Delta G_{com}$ quantities can be used for the prediction of inhibitory potencies K_i^{pre} against the DHQ2 of *M. tuberculosis* for novel AQ analogues provided that they share the same binding mode of the training set of 3-dehydroquinic acid ligands. To identify chemical modifications of AQs leading to new inhibitor structures with high predicted binding affinity to *MtDHQ2*, we have analysed the contributions of individual residues of the enzyme binding pocket to the total computed enzyme-inhibitor interaction energy (E_{int}). In this respect we noticed an important contribution to E_{int} from residues Asn12, Leu13, Tyr24, Hisd101, Ser103, and Arg112.

3.2. Binding mode of inhibitors

Besides the robustness of QSAR model, the analysis of the interactions between AQs and *MtDHQ2* is expected to reveal key interactions justifying AQx:*MtDHQ2* affinities such as van der Waals (VdW) contact, hydrogen bond (HB) and hydrophobic contacts. As displayed in **Figure 4** the binding mode of AQs at *MtDHQ2* active site of the best active AQ1 in 2D and 3D is supported by the following interactions in the binding site; H-bond with Ser203, Ile102 and His101, along with π - π interactions with Tyr24. The carboxyl group is binding to backbone amide of Ile102 and Ser103, C-1 hydroxyl is binding to Hisd101 which acts as proton donor in enzymatic mechanism of *MtDHQ2*, and apparent hydrogen binding between carbonyl group of cyclohexane and side chain of Asn12. The aromatic moiety of inhibitors is in close contact with the side chain of residues Leu13, Leu16, Arg15, Ile102, and Tyr24, establishing important lipophilic interactions. Precisely, the aromatic ring interacts by π -stacking with the side

chain of Tyr24. This interaction is relevant and is probably the main driving force of an increase of affinity of the inhibitors (Erreur ! Source du renvoi introuvable.; AQ1-2). Electrostatic interaction between benzyl fragment and Arg19 which is an essential residue for enzyme activity is associated with previous observations.

A comparison of the interaction patterns (Erreur ! Source du renvoi introuvable.and Erreur ! Source du renvoi introuvable.) highlights the main stabilizing contributions of individual residues to the total interaction energy E_{int} of *MtDHQ2*:AQ for the highly active AQs (hAQs) explicitly AQ1 (0.026 μ M) and AQ2 (0.028 μ M) (fig. 6) and for less active ones (lAQs) AQ13 (20 μ M) and AQ14 (15 μ M) (fig.7). These contributions expressed in % of E_{int} for hAQs vs. lAQs for Asn12 (9% vs.6%), Arg15 (3% vs.0%), Leu16 (4% vs. 3%), Arg19 (5% vs.2%), Glu20 (2% vs. -1%), Tyr24 (16% vs.13%) and Arg108 (1% vs.-1.5%) are essential to the binding of potent inhibitors. A refined analysis of hAQs (Erreur ! Source du renvoi introuvable.) reveals the important contributions of two catalytic residues (Arg19, Tyr24). A larger aryl ring increases slightly the π - π interaction with Tyr24 (15% for AQ1 and 15.5% for AQ2, Erreur ! Source du renvoi introuvable.). In addition, fragment for which the electrostatic interaction with Arg19 can be improved results in enhancing the binding affinity (5% AQ1 (26 nM) vs. 3% AQ2 (28 nM)).

3.3. New analogues

The new analogues are derived from the most potent training set inhibitor AQ1 (Table 1) are intended to involve residues Asn12, Arg19 and Tyr24 upon inhibitor binding. The top virtual hits are AQ-38-02, AQ-38-16, AQ-38-17, AQ-38-20, AQ-38-21, AQ-38-40 (Table 7). They possess large aryl moiety in position (R1; epimer R) which interacts with catalytic Tyr24 increasing hydrophobic contact to a better stabilization and greater affinity. The best of them, AQ38-02 reached predicted inhibitory potency towards *MtDHQ2* K_i^{pre} = 0.25 nM (Table 7). This best analogue AQ38-02 involves strong interactions with the

above-mentioned residues (Figure 11). As an illustration, we can mention σ - π interaction between the side chain of Asn12 and aromatic ring moiety, π - π interaction between the side chain of Tyr24 and aromatic ring moiety and, hydrogen bonding between Arg19 and the oxygen atom of this fragment. In the position R2, the fluorine atom establishes Hydrogen bonding interaction with residue Asn12. These interactions intensified the affinity towards *Mt*DHQ2.

The ADME related properties described in Section 2.8 were computed for the forty (40) newly designed AQs inhibitors of DHQ2 and antituberculosis either in clinical use or in clinical trials with QikProp software [39]. About Thirty of these new analogues have their drug-likeness parameter (#stars) which characterizes the ADME related properties relevant for the pharmacokinetic profile of a compound equal to zero. Thus the designed AQs analogues are predicted to possess favorable pharmacokinetic profiles and represent suitable candidates for synthesis and experimental evaluation.

Table 7. Predicted ADME-related properties of the best AQs analogues (6) and known antitubercotics either in use or in test computed by QikProp [34]. (*) Star indicating that the property descriptor value falls

Name	#stars ^a	Mw ^b	S _{mol} ^c	S _{mol,hfo} ^d	V _{mol} ^e	RotB ^f	HB _{don} ^g	HB _{acc} ^h	logP _{ow} ⁱ	logS _{wat} ^j	logK _{HSA} ^k	logB/B ^l	BIP _{caco} ^m	#metab ⁿ	K _p ^{predo} [nM]	HOA ^o	%HOA ^q	Stereo
AQ-38-02	0	355	555	232	1014	8	5	8.4	-1.2	-2.0	-0.6	-1.1	9.1	6	0.25	2	37	2R,3R
AQ-38-21	0	407	658	358	1243	11	5	8.4	0.0	-2.8	-0.3	-1.5	8.4	6	0.43	2	43	2R,3R
AQ-38-16	0	394	627	325	1178	10	5	10.4	-1.6	-1.0	-0.6	-1.0	2.0	7	0.44	1	23	2R,3S
AQ-38-40	0	505	747	261	1442	13	6	9.9	0.2	-2.4	-0.3	-1.2	1.9	8	0.47	1	7	2R,3R
AQ-38-20	0	393	629	328	1189	10	5	8.4	-0.3	-2.5	-0.4	-1.4	8.4	6	0.61	2	41	2R,3R
AQ-38-17	0	379	600	301	1130	10	5	8.4	-0.7	-2.1	-0.5	-1.4	8.5	6	0.85	2	40	2R,3R
Rifampicin	1	137	313	0.0	479*	2	3	4.5	-0.7	0.0	-0.8	-0.8	267.5	2	-	2	67	-
Isoniazid	4	123*	299	0.0	442*	1	2	5	-0.6	-0.5	-0.8	-0.7	298.4	4	-	2	67	-
Ethambutol	2	204	476	396	805	11	4	6.4	-0.2	0.6	-0.8	0.0	107.8	4	-	2	62	-
Pyrazinamide	10	823*	1090*	850*	2300*	25*	6	20.3*	3.0	-3.1	-0.3	-2.7	38.2	11*	-	1	34	-
Gatifloxacin	0	375	597	356	1093	2	1	6.8	0.5	-4.0	0.0	-0.6	17.0	1	-	2	52	-
Moxifloxacin	0	401	641	396	1167	2	1	6.8	1.0	-4.7	0.2	-0.6	20.9	1	-	2	56	-
Rifapentine	10	877	1024*	845*	2332*	24*	6	20.9*	3.6	-2.2	-0.2	-1.5	224.0	13*	-	1	51	-
Bedaquiline	4	556	786	214	1531	9	1	3.8	7.6*	-6.9	1.7	0.4	1562.2	5	-	1	100	-
Delamanid	2	535	796	284	1469	7	0	6.0	5.8	-7.6	1.0	-1.0	590.9	2	-	1	85	-
Linezolid	0	337	555	337	995	2	1	8.7	0.6	-2.0	-0.7	-0.5	507.0	2	-	3	79	-
Sutezolid	1	353	594	331	1046	2	1	7.5	1.3	-3.4	-0.4	-0.4	449.3	0	-	3	82	-
Ofloxacin	1	361	581	337	1044	1	0	7.3	-0.4	-2.8	-0.5	-0.4	25.9	1	-	2	50	-
Amikacin	14	586	738	351	1499	22*	17*	26.9*	-7.9*	-0.2	-2.1	-3.5	0.0	14*	-	1	0	-
Kanamycin	10	485	656	259	1290	17*	15*	22.7*	-6.7*	2.0	-1.4	-3.1	0.0	12*	-	1	0	-
Imipenem	0	299	487	259	879	8	3	7.2	1.0	-1.8	-0.7	-1.4	35.0	3	-	3	61	-
Amoxicillin	2	365	561	165	1032	6	4.25	8.0	-2.5	-0.8	-1.1	-1.5	1.0	5	-	1	12	-
clavulanate	0	199	396	185	629	4	2	6.5	-0.8	0.3	-1.3	-1.3	13.3	2	-	2	42	-

[a] Drug likeness number of property descriptors (from 24 out of the full list of 49 descriptors of QikProp, ver. 3.3) range for 95% of known drugs [0-5];

[b] Molecular weight [$g.mol^{-1}$], (range for 95% of drugs: 130 – 725Da) (57);

[c] Total solvent-accessible molecular surface. In \AA^2 (probe radius 1.4 \AA) (range for 95% of drugs: 300 – 1000 \AA^2);

[d] Hydrophobic portion of the solvent-accessible molecular surface. In \AA^2 (probe radius 1.4 \AA) (range for 95% of drugs: 0 – 750 \AA^2);

[e] Total volume of molecule enclosed by solvent-accessible molecular surface. In \AA^3 (probe radius 1.4 \AA) (range for 95% of drugs: 500 – 2000 \AA^3);

[f] Number of rotatable bonds (range for 95% of drugs: 0 – 15);

[g] Number of hydrogen bonds donated by the molecule (range for 95% of drugs: 0 – 6);

[h] Number of hydrogen bonds accepted by the molecule (range for 95% of drugs: 2 – 20);

[i] Logarithm of partitioning coefficient between n-octanol and water phases (range for 95% of drugs: -2 – 6.5);

[j] Logarithm of aqueous solubility (range for 95% of drugs: -6.0 – 0.5);

[k] Logarithm of predicted binding constant to human serum albumin (range for 95% of drugs: -1.5 – 1.5);

[l] Logarithm of predicted blood/brain barrier partition coefficient (range for 95% of drugs: -3.0 – 1.2);

[m] Predicted apparent Caco-2 cell membrane permeability in Boehringer-Ingelheim scale. In [nm/s] (range for 95% of drugs: <5 low.> 100 high);

[n] Number of likely metabolic reactions (range for 95% of drugs: 1 – 8);

[o] Predicted K_p^{pred} were estimated from the QSAR equation (B) shown in Table;

[p] Human oral absorption (1 - low. 2 - medium. 3 - high);

[q] Percentage of human oral absorption in gastrointestinal tract (<25% - poor.>80% high).

5. CONCLUSIONS

The QSAR model for reversible inhibition of MtDHQ2 based on the correlation between inhibitors experimental activities and the computed Gibbs free energy of enzyme-inhibitor interactions for complexes AQx:DHQ2 was validated by cross checking with the PH4 pharmacophore model derived from a training set of AQs. The statistical significance of the QSAR and PH4 pharmacophore models derived from a training set of 14 AQ and a validation set of 3 AQ [21] compounds was well documented. The analysis of the binding mode of inhibitors and the active site residue contributions to E_{int} directed our efforts to optimize the structures of the known inhibitors and enhance the involvement of the residues Asn12, Arg19 and Tyr 24 upon inhibitor binding. We have then replaced in the cyclohexane scaffold of most potent training set inhibitor AQ1, forty various moieties in positions R1 and R2. The derived compounds which possess large aromatic moiety in position R1 (C2) improved the binding site interactions by pi-interaction involving Asn12 (σ - π), Tyr 24 (π - π) and hydrogen bonding involving the Asn12 and Arg19 residues. The best analogue designed, which is 100 times more potent than the best training set inhibitor AQ1, namely AQ-38-02, with predicted potency $K_i^{\text{pred}} = 0.25$ nM may be proposed for synthesis and subsequent activity evaluation in enzymatic assays, with emphasis serve as a lead compound for the discovery of novel antituberculotics.

ACKNOWLEDGEMENTS

FNK acknowledges a return fellowship and equipment subsidy from the Alexander von Humboldt Foundation, Germany. LCOO acknowledges with thanks a financial support from the University of Yaoundé I for a research stay at the University Nangui Abrogoua, Ivory Coast.

The authors thank Eugene Megnassan for helpful advice.

Conflicts of interest

The authors declare no competitive conflicts of interest.

REFERENCES

- [1] World Health Organization (WHO). (2015) Global Tuberculosis; WHO: Geneva, Switzerland.
- [2] World Health Organization (WHO). (2020) Global Tuberculosis; WHO: Geneva, Switzerland.
- [3] van Sumere, C. F.; Lea, P. J. (Eds.) (1985) the biochemistry of plant phenolics. Annual Proceedings of the Phytochemical Society, vol. 25. Oxford: Clarendon Press; .
- [4] Abell, C. (1998) Enzymology and molecular biology of the shikimate pathway. In: Sankawa U (Ed.) Comprehensive natural products chemistry. Oxford: Pergamon, Elsevier Science Ltd., pp. 573-607. [View Article](#)
- [5] Bentley R. (1990) The shikimate pathway-A metabolic tree with branches. Crit. Rev. Biochem. Mol. Biol., 25, 307-383. PMID:2279393 [View Article](#) [PubMed/NCBI](#)
- [6] Herrmann, K.; Weaver, L. (1999) The shikimate pathway. Annu. Rev. Plant Physiol. Plant Mol. Biol., 50, 473-755. PMID:15012217 [View Article](#) [PubMed/NCBI](#)
- [7] Gibson, F.; Pittard, A. J. (1968) Pathways of biosynthesis of aromatic amino acids and vitamins and their control in microorganisms. Bacteriol Rev. , 32, 465-492. PMID:4884716 [View Article](#) [PubMed/NCBI](#)
- [8] Harris, J.; González-Bello, C.; Kleanthous, C.; Coggins, J. R.; Hawkins, A. R.; Abell, C. (1996) Evidence from kinetic isotope studies for and enolate intermediate in the mechanism of type II dehydroquinases. Biochem. J., 319, 333-336. PMID:8912664 [View Article](#) [PubMed/NCBI](#)
- [9] Krell, T.; Pitt, A. R.; Coggins, J. R. (1995) The use of electrospray mass spectrometry to identify an essential arginine residue in type II dehydroquinases. FEBS Lett, 360, 93-96. 00083-L [View Article](#)
- [10] Krell, T.; Horsburgh, M. J.; Cooper, A.; Kelly, S. M.; Coggins, J. R. (1996) Localization of the active site of type II dehydroquinase. Identification of a common arginine containing motif in the two classes of dehydroquinases. J. Biol. Chem. , 271, 24492-24497. PMID:8798709 [View Article](#) [PubMed/NCBI](#)
- [11] Lence E, Marc W. , González-Bello C., Mulholland A.J.M. (2018) QM/MM simulations identify the determinants of catalytic activity differences between type II dehydroquinase enzymes , Org. Biomol. Chem., 16, 4443 PMID:29767194 [View Article](#) [PubMed/NCBI](#)
- [12] Roszak, A. W.; Robinson, D. A.; Krell, T.; Hunter, I. S.; Fredrickson, M.; Abell, C.; Coggins, J. R.; Lapthorn, A. (2002) J. The structure

- and mechanism of the type II dehydroquinase from *Streptomyces coelicolor*. *Structure*, 10, 493-503. 00747-5 [View Article](#)
- [13] Peón, A.; Otero, J. M.; Tizón, L.; Prazeres, V. F.; Llamas-Saiz, A. L.; Fox, G. C.; van Raaij, M. J.; Lamb, H.; Hawkins, A. R.; Gago, F.; Castedo, L.; González-Bello, C. (2010) Understanding the key factors that control the inhibition of type II dehydroquinase by (2R)-2-benzyl-3-dehydroquinic acids. *Chem Med Chem*, 5, 1726-1733. PMID:20815012 [View Article](#) [PubMed/NCBI](#)
- [14] Tizón, L.; Otero, J. M.; Prazeres, V. F.; Llamas-Saiz, A. L.; Fox, G. C.; van Raaij, M. J.; Lamb, H.; Hawkins, A. R.; Ainsa, J. A.; Castedo, L.; González-Bello, C. (2011) A Prodrug approach for improving antituberculosis activity of potent *Mycobacterium tuberculosis* type II dehydroquinase inhibitors. *J. Med. Chem.*, 54, 6063-6084. PMID:21780742 [View Article](#) [PubMed/NCBI](#)
- [15] Coderch, C., Lence E., Peón A., Lamp H., Hawkins A. R. et al. (2014), Mechanistic insight into the reaction catalysed by bacterial type II dehydroquinases, *Biochem. J.* (2014) 458, 547-557 PMID:24392963 [View Article](#) [PubMed/NCBI](#)
- [16] González-Bello, C. (2016) Inhibition of Shikimate Kinase and Type II Dehydroquinase for Antibiotic Discovery: Structure-Based Design and Simulation Studies, *Current Topics in Medicinal Chemistry*, 16, 960-977 PMID:26303426 [View Article](#) [PubMed/NCBI](#)
- [17] González-Bello, C.; Castedo, L. (2007) Progress in type II dehydroquinase inhibitors: from concept to practice. *Med. Res. Rev.*, 27, 177-208. PMID:17004270 [View Article](#) [PubMed/NCBI](#)
- [18] Howard, N. I.; Dias, M. V.; Peyrot, F.; Chen, L.; Schmidt, M. F.; Blundell, T. L.; Abell, C. (2015) Design and structural analysis of aromatic inhibitors of type II dehydroquinase from *Mycobacterium tuberculosis*. *ChemMedChem*, 10, 116-133. PMID:25234229 [View Article](#) [PubMed/NCBI](#)
- [19] Lence, E.; Tizón, L.; Otero, J. M.; Peón, A.; Prazeres, V. F.; Llamas-Saiz, A. L.; Fox, G. C.; van Raaij, M. J.; Lamb, H.; Hawkins, A. R.; González-Bello, C. Mechanistic basis of the inhibition of type II dehydroquinase by (2S)- and (2R)-2-benzyl-3-dehydroquinic acids. *ACS Chem. Biol.*, 8, 568-577. PMID:23198883 [View Article](#) [PubMed/NCBI](#)
- [20] Blanco B, Sedes S, Peón A., Lamp H., Hawkins A. R. et al. (2012) Synthesis of 3-alkyl enol mimics inhibitors of type II dehydroquinase: factors influencing their inhibition potency, *Org. Bio-mol. Chem.*, 10, 3662 -3676 PMID:22447158 [View Article](#) [PubMed/NCBI](#)
- [21] González-Bello, C. (2016) Inhibition of shikimate kinase and Type II dehydroquinase for antibiotic discovery: structure-based design and simulation studies. *Curr. Top. Med. Chem.*, 16, 960-977. PMID:26303426 [View Article](#) [PubMed/NCBI](#)
- [22] Prazeres, V. F.; Castedo, L.; Lamb, H.; Hawkins, A. R.; González-Bello, C. 2 substituted-3-dehydroquinic acids as potent competitive inhibitors of type II dehydroquinase. *ChemMedChem*, 2009, 4, 1980-1984. PMID:19856378 [View Article](#) [PubMed/NCBI](#)
- [23] Frecer, V.; Kabelac, M.; De Nardi, P.; Pricl, S.; Miertus (2004) Structure-based design of inhibitors of NS3 serine protease of hepatitis C virus. *J. Mol. Graph. Model.* 2004, 22, 209-220. 00161-X [View Article](#)
- [24] Frecer, V.; Jedinak, A.; Tossi, A.; Berti, F.; Benedetti, F.; Romeo, D.; Miertus, S. Structure based design of Inhibitors of aspartic protease of HIV-1. *Lett. Drug. Des. Discov.*, 2, 638-646. [View Article](#)
- [25] Frecer, V.; Berti, F.; Benedetti, F.; Miertus, S. (2008) Design of peptidomimetic inhibitors of aspartic protease of HIV-1 containing-PheΨPro-core and displaying favourable ADME-related properties. *J. Mol. Graph. Model.*, 27, 376-387. PMID:18678515 [View Article](#) [PubMed/NCBI](#)
- [26] Dali, B.; Keita, M.; Megnassan, E.; Frecer, V.; Miertus, S. (2012) Insight into selectivity of peptidomimetic inhibitors with modified statine core for plasmepsin II of *Plasmodium falciparum* over human cathepsin D. *Chem. Biol. Drug Des.*, 79, 411-430. PMID:22129033 [View Article](#) [PubMed/NCBI](#)
- [27] Megnassan, E.; Keita, M.; Bieri, C.; Esmel, A.; Frecer, V.; Miertus, S. (2012) Design of novel dihydroxynaphthoic acid inhibitors of *Plasmodium falciparum* lactate dehydrogenase. *Med. Chem.*, 8, 970-984. PMID:22741776 [View Article](#) [PubMed/NCBI](#)
- [28] Owono, L. C. O.; Keita, M.; Megnassan, E.; Frecer, V.; Miertus, S. (2013,) Design of thymidine analogues targeting thymidilate kinase of *Mycobacterium tuberculosis*. *Tubercul. Res. Treatment.*, 2013, 670836. PMID:23634301 [View Article](#) [PubMed/NCBI](#)
- [29] Keita, M.; Kumar, A.; Dali, B.; Megnassan, E.; Siddiqi, M. I.; Frecer, V.; Miertus, S. (2014) Quantitative structure-activity relationships and design of thymine-like inhibitors of thymidine monophosphate kinase of *Mycobacterium tuberculosis* with favourable pharmacokinetic profiles. *RSC Adv.*, 4, 55853-55866. [View Article](#)

- [30]Freceer, V.; Seneci, P.; Miertus, S. (2011) Computer-assisted combinatorial design of bicyclic thymidine analogues as inhibitors of Mycobacterium tuberculosis thymidine monophosphate kinase. *J. Comput-Aided Mol. Des.*, 25, 31- 49. PMID:21082329 [View Article](#) [PubMed/NCBI](#)
- [31]Owono, L. C. O.; Ntie-Kang, F.; Keita M., Megnassan, E.; Freceer, V.; Miertus, S. (2015) virtually designed triclosan based inhibitors of enoyl-acyl carrier protein reductase of Mycobacterium tuberculosis and of Plasmodium falciparum. *Mol. Inf.*, 34, 292-307. PMID:27490275 [View Article](#) [PubMed/NCBI](#)
- [32]Kouassi, F.; Kone, M.; Keita, M.; Esmel, A.; Megnassan, E.; Freceer, V.; N'Guessan, T.; Miertus, S. (2015) Computer-aided design of orally bioavailable pyrrolidine carboxamide inhibitors of enoyl-acyl carrier protein reductase of Mycobacterium tuberculosis with favorable pharmacokinetic profiles. *Int. J. Mol. Sci.*, 16, 29744-29771. PMID:26703572 [View Article](#) [PubMed/NCBI](#)
- [33]N'Guessan, H.; Megnassan, E. (2017) In silico design of phosphonic arginine and hydroxamic acid inhibitors of Plasmodium falciparum M17 leucyl aminopeptidase with favorable pharmacokinetic profile. *J. Drug. Design Med. Chem.*, 3, 86-113. [View Article](#)
- [34]Kily, Y. H. F.; Toi, B.; Megnassan, E.; Freceer, V.; Miertus, S. (2018) In silico design of Plasmodium falciparum cysteine protease falcipain 2 inhibitors with favorable pharmacokinetic profile. *J. Anal. Pharm. Res.*, 7, 298-309. [View Article](#)
- [35]Fischer, S.; Smith, A. J. C.; Verma, C. S. (2001) Dissecting the vibrational entropy change on protein/ligand binding: Burial of a water molecule in bovine pancreatic trypsin inhibitor. *J. Phys. Chem. B.*, 105, 8050-8055. [View Article](#)
- [36]Schwarzl, S. M.; Tschopp, T. B.; Smith, J. C.; Fischer, S. (2002) Can the calculation of ligand binding free energies be improved with continuum solvent electrostatics and an ideal-gas entropy correction? *J. Comput. Chem.*, 23, 1143-1149. PMID:12116383 [View Article](#) [PubMed/NCBI](#)
- [37]Discovery Studio Molecular Modeling and Simulation Program; Version 2.5; Accelrys, Inc.: San Diego, CA, USA, (2009).
- [38]Maple, J. R.; Hwang, M.-J.; Stockfish, T. P.; Dinur, U.; Waldman, M.; Ewig, C.; Hagler, A. (1994) Derivation of class II forcefields I: methodology and quantum forcefield for the alkyl functional group and alkane molecules. *J. Comput. Chem.*, 15, 162-182. [View Article](#)
- [39]QikProp, version 3.7, release 14, X Schrödinger, LLC, New York, NY, (2014)
- [40]Duffy E. M.; Jorgensen, W. L. (2000) Prediction of properties from simulations: free energies of solvation in hexadecane, octanol, and water. *J. Am. Chem. Soc.*, 122, 2878-2888. [View Article](#)
- [41]Molecular Operating Environment (MOE), 2014.10, Chemical Computing Group Inc., Montreal, QC, Canada, H3A 2R7, 2014
- [42]Available Chemicals Directory, Version 95.1, MDL Information Systems, San Leandro, CA.